DOI 10.1007/s11595-016-1447-z

Fabrication of $BiVO_4$: Effect of Structure and Morphology on Photocatalytic Activity and Its Methylene Blue Decomposition Mechanism

GUO Minna, HE Qianglong, WANG Wenjie, WU Jie, WANG Weimin*

(State Key Laboratory of Advanced Technology for Materials Synthesis and Processing, Wuhan University of Technology, Wuhan 430070, China)

Abstract: $BiVO_4$ photocatalysts were synthesized by a surfactant free hydrothermal method without any further treatments, and characterized by X-ray diffraction (XRD), scanning electron microscopy (SEM), transmission electron microscopy (TEM), ultraviolet-visible diffuse reflectance spectroscopy (UV-vis DRS), Raman spectroscopy, and Brunauer-Emmett-Teller (BET) surface area techniques. The photocatalytic activity was evaluated for the degradation of the methylene blue (MB) under visible light irradiation. Seen from the structural and morphological characterization, it is stated that the obtained samples present monoclinic phase, and the pH value has significant influence on the morphologies. The enhanced photocatalytic performance was associated with its crystallinity, unique morphology, band gap energy, BET specific surface area, surface charge and adsorption capacity. The recycle experiments results show that the $BiVO_4$ photocatalysts have excellent photo-stability, and we deduced a possible mechanism by examining the effects of the active species involved in the photocatalytic process for MB photocatalytic degradation.

Key words: $BiVO_4$; morphology; photocatalytic; methylene blue; dcomposition mechanism

1 Introduction

Bismuth vanadate ($BiVO_4$) is a promising photocatalyst because of its properties such as non-toxicity, high stability, and excellent photocatalytic effect in organic dye degradation[1-6]. It has three crystalline phases[7-12]: monoclinic-scheelite, tetragonal-zircon, and tetragonal-scheelite. Among the three crystalline phases, the monoclinic-scheelite structure shows the best photocatalytic activity under visible-light irradiation because of its narrower band gap (2.4 eV)[13-15] than that of tetragonal structure (2.9 eV)[7]. The investigation results indicate that the photocatalytic activities of monoclinic- scheelite $BiVO_4$ strongly rely on their crystallinity, sizes, structures, and morphologies[16-23]. Therefore, the synthesis of $BiVO_4$ with controllable morphology is desirable. Efforts have been made to achieve controllable synthesis of $BiVO_4$ structures for enhanced photocatalytic performances. For example, Obregón S *et al*[24] reported the fabrication of various shaped monoclinic $BiVO_4$ materials by a surfactant free hydrothermal method, and they set the pH at 5 and 9 by adding NH_4OH or triethylamine (TEA) as pH controlling agent. They found that the morphology of $BiVO_4$ systems was notably affected by the pH of the precipitation, and the best photocatalytic performance was attained by the samples with needle-like morphology. Yu *et al*[25] synthesized highly crystalline monoclinic scheelite $BiVO_4$ powders over a wide range of pH by a hydrothermal process, and the local structure, as well as the crystallinity, provided a significant effect on the photocatalytic performance for O_2 evolution under visible-light irradiation. Ai *et al*[26] synthesized hierarchical monoclinic $BiVO_4$ three-dimensional (3D) superstructures with microboats and microspheres morphologies by a hydrothermal method using ethylene glycol as solvent. They found that the $BiVO_4$ microspheres showed superior photocatalytic activity on removal of gaseous NO compared to the $BiVO_4$ microboats, and the morphology-dependent photocatalytic property of the $BiVO_4$ superstructures is related to loosely packed hierarchical morphology

(Received: June 5, 2015; Accepted: Aug. 4, 2015)

GUO Minna(郭敏娜): Ph D Candidate;E-mail: guomn_007@126.com

* Corresponding author: WANG Weimin(王为民): Prof.; E-mail:wangwm@hotmail.com

Funded by the National Science Foundation of China (U12301013) and the National Science Foundation of China (51521001)

with larger surface area. Despite the fact that $BiVO_4$ photocatalysis research has been flourished for a long time, detailed studies on the influences of accurate pH values upon the photocatalytic activity and photodegradation mechanism have still been limited.

In this study, we successfully synthesized $BiVO_4$ with controlled morphology by adjusting the pH values using $NH_3 \cdot H_2O$ for the photocatalytic oxidation of MB under visible light irradiation by a hydrothermal method without any surfactants or further treatments. The relationship between pH values of precursors and the morphology, size, crystallinity, band gap energy, and specific surface area of powder, and the influences of these factors on the photocatalytic activities of synthetic $BiVO_4$ samples have been investigated. The cycling stabilities of the prepared $BiVO_4$ photocatalysts were investigated. To deeply understand the MB decomposition mechanism of the $BiVO_4$ system, we detected the active species involved in photocatalytic degradation.

2 Experimental

2.1 Catalyst preparation

In a typical synthesis procedure, 5 mmol $Bi(NO_3)_3 \cdot 5H_2O$ was dissolved in 25 mL acetic acid (36%) under magnetic stirring for 30 min at room temperature to form solution A; 5 mmol NH_4VO_3 was dissolved in 25 mL deionized water under magnetic stirring for 30 min at 70 ℃ to form solution B. Solution B was added dropwise into solution A under stirring. The pH value was adjusted to 1.68, 3.14, 4.94, 6.87, and 9.18 using $NH_3 \cdot H_2O$ solution. Subsequently, the mixture was transferred to a 100 mL Teflon-lined autoclave, and maintained at 180 ℃ for 15 h, and then cooled naturally to room temperature. The precipitates were filtered, repeatedly washed, and dried overnight at 60 ℃.

The samples' names are denoted by Nx based on the different pH values, for example, N3.14 particularly refers to the sample produced at pH value of 3.14.

2.2 Characterization

The crystal structures of the photocatalysts were determined by X-ray diffraction (XRD; Rigaku Ultima Ⅲ, Japan). The morphologies were investigated by scanning electron microscopy (SEM; Hitachi S-3400N Ⅱ, Japan) and transmission electron microscopy (TEM, JEM2100F, Japan). Ultraviolet-visible diffuse reflectance spectra (UV-vis DRS) were collected using a UV-vis spectrometer (Shimadzu UV-2550, Japan) with $BaSO_4$ as a reference. The Brunauer-Emmett-Teller (BET) specific surface areas (S_{BET}) were obtained from N_2 adsorption-desorption isotherms determined at liquid N_2 temperature on an automatic analyzer (ASAP 2020M, USA). The visible light Raman spectra were recorded by a RENISHAW Raman microscope (INVIA, China) using 525 nm lasers. The surface charge was determined by electrophoretic mobility using a Zeta potential analyzer (ZetaPALS, USA).

2.3 Photocatalytic activity

The photocatalytic activities of the samples were evaluated based on MB decolorization, using a 350 W Xe-illuminator as the light source. A 420 nm cut-off filter was placed between the Xe-illuminator and the reactor. The powder (0.1 g) was added to 100 mL of MB solution with a concentration of 10 mg/L. The solution was stirred in the dark for 60 min to achieve adsorption-desorption equilibrium between the MB molecules and catalyst particles prior to light irradiation. At various irradiation time intervals, 3 mL suspensions were collected, and centrifuged to remove the photocatalyst particles. The concentrations of the remnant MB were then monitored using a UV-vis spectrometer (Shimadzu UV-2550) at a wavelength of 665 nm.

3 Results and discussion

3.1 XRD analysis

Fig.1 shows the XRD patterns of the $BiVO_4$ samples synthesized at different pH values. The diffraction peaks of all the samples can be well indexed to the pure monoclinic phase of $BiVO_4$ (JCPDS card No. 14-0688). It is worth noting that the relative intensities of the diffraction peaks I_{040}/I_{121} increase obviously with increasing pH values, which indicates a preferred (040) surface orientation of the $BiVO_4$ crystal growth.

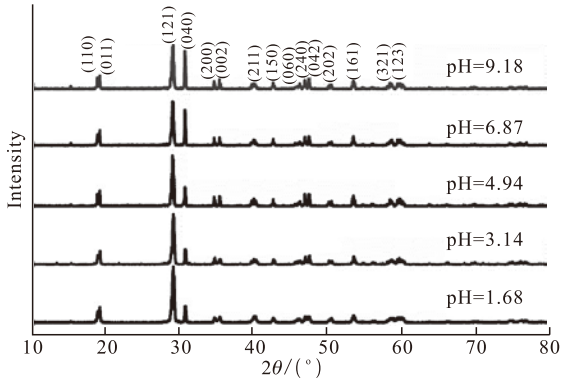

Fig.1 XRD patterns of the $BiVO_4$ samples synthesized at different pH values

Table 1 Some selected properties of $BiVO_4$ samples

Samples	Crystalline size/nm	Bandgap/eV	S_{BET}/($m^2 \cdot g^{-1}$)	FWHM(Raman)	Zeta potential/mV	Adsorption capability/%
N1.68	23.89	2.48	3.87	55.388	–25.71	0.3
N3.14	25.77	2.46	4.28	55.406	–27.94	3.7
N4.94	26.29	2.45	5.01	58.66	–30.43	4.9
N6.87	29.33	2.43	2.31	61.926	–47.53	8.2
N9.18	30.35	2.44	1.49	68.446	–38.01	6.1

The average sizes of the crystallites with the (121) peak were calculated using the Scherrer equation ($D = K\lambda/(\beta\cos\theta)$), where K is 0.89, λ is the X-ray wavelength (0.154 nm), β is the full width at half maximum, and θ is the half of the diffraction angle. The crystal sizes calculated from the (121) peaks increase as pH value increases, varying from 23.89 to 30.35 nm, as shown in Table 1, from which we deduced that the sample crystallinity improved as pH value increased[27].

3.2 Raman spectra

For probing the local structure of prepared $BiVO_4$ samples, Raman spectroscopy was used, the results are presented in Fig.2, from which we can see that the spectra include a single major band at around 820 cm^{-1}, normally assigned to the symmetric V-O stretching mode (*eg*, Ag symmetry). The positions and the full width at half maximum (FWHM) of the most intensive bands near 820 cm^{-1} were determined using Lorentzian-type curve fitting. As pH values increase, these Raman bands shift towards the lower end of wavenumber gradually, *i e*, from 818.9 to 812.3 cm^{-1}, indicating that the V-O bond length becomes longer, meaning the increase of crystallinity[28]. Besides, the FWHM values of these Raman bands increase as pH values increase, as shown in Table 1. It is known that the Raman widths are sensitive to the degree of crystallinity, defects and structural disorders[29,30]. Therefore, the Raman results indicate that the higher pH samples have better crystallinity and contained less defects than samples prepared at lower pH conditions, which is in agreement with the XRD results.

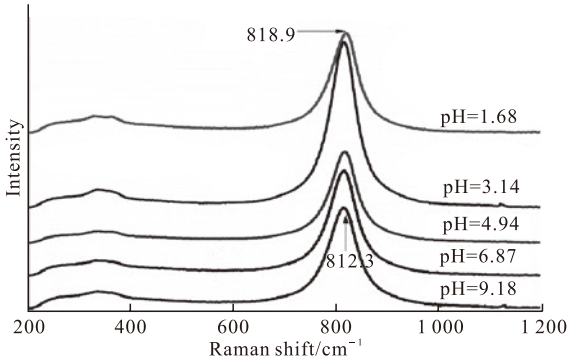

Fig.2 Raman spectra of the $BiVO_4$ samples synthesized at different pH values

3.3 Morphologies of $BiVO_4$ samples

The micrographs of the $BiVO_4$ samples prepared at different pH values were observed by SEM, as shown in Fig.3. It is seen that pH values have significant influence on the samples morphologies. The sample synthesized at pH = 1.68 (Fig.3(a)) possesses a wax gourd structure formed by small crystals. As pH increases, the morphology changes drastically. When pH = 3.14, peanut-like aggregates formed (Fig.3 (b)). when the pH value increases further to 4.94, the peanut-like shape seems to collapse to form loose hierarchical structure and particles (Fig.3(c)). The morphology collapses thoroughly to particles when pH = 6.87 (Fig.3(d)). At higher pH, the particles grew into needle-like ones (Fig.3(e)).

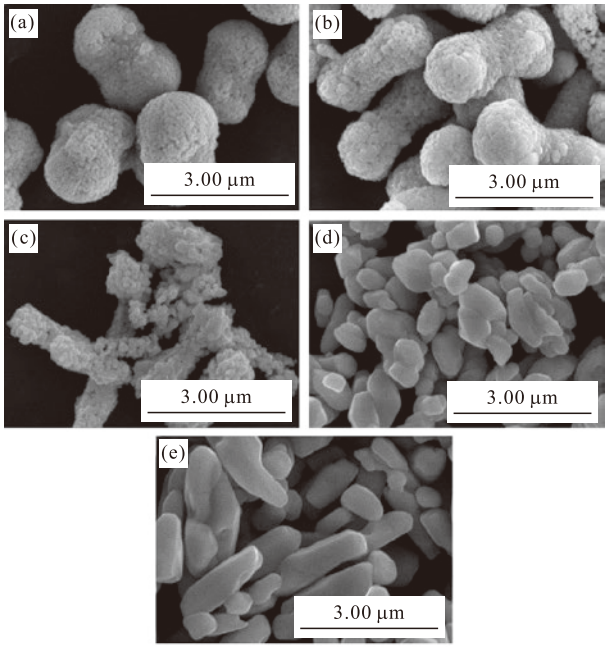

Fig.3 Typical SEM images of the $BiVO_4$ samples synthesized at different pH values: (a) pH = 1.68; (b) pH = 3.14; (c) pH =4.94; (d) pH = 6.87; (e) pH = 9.18

In the present synthesis, low pH value inhibited $Bi(NO_3)_3 \cdot 5H_2O$ to hydrolyze, leading to fewer $BiVO_4$ crystal nuclei be formed in the precursor solutions. When $NH_3 \cdot H_2O$ was added, it would consume H^+, which benefited to increase the amount of $BiVO_4$ crystal nuclei, so $NH_3 \cdot H_2O$ could determine the concentration

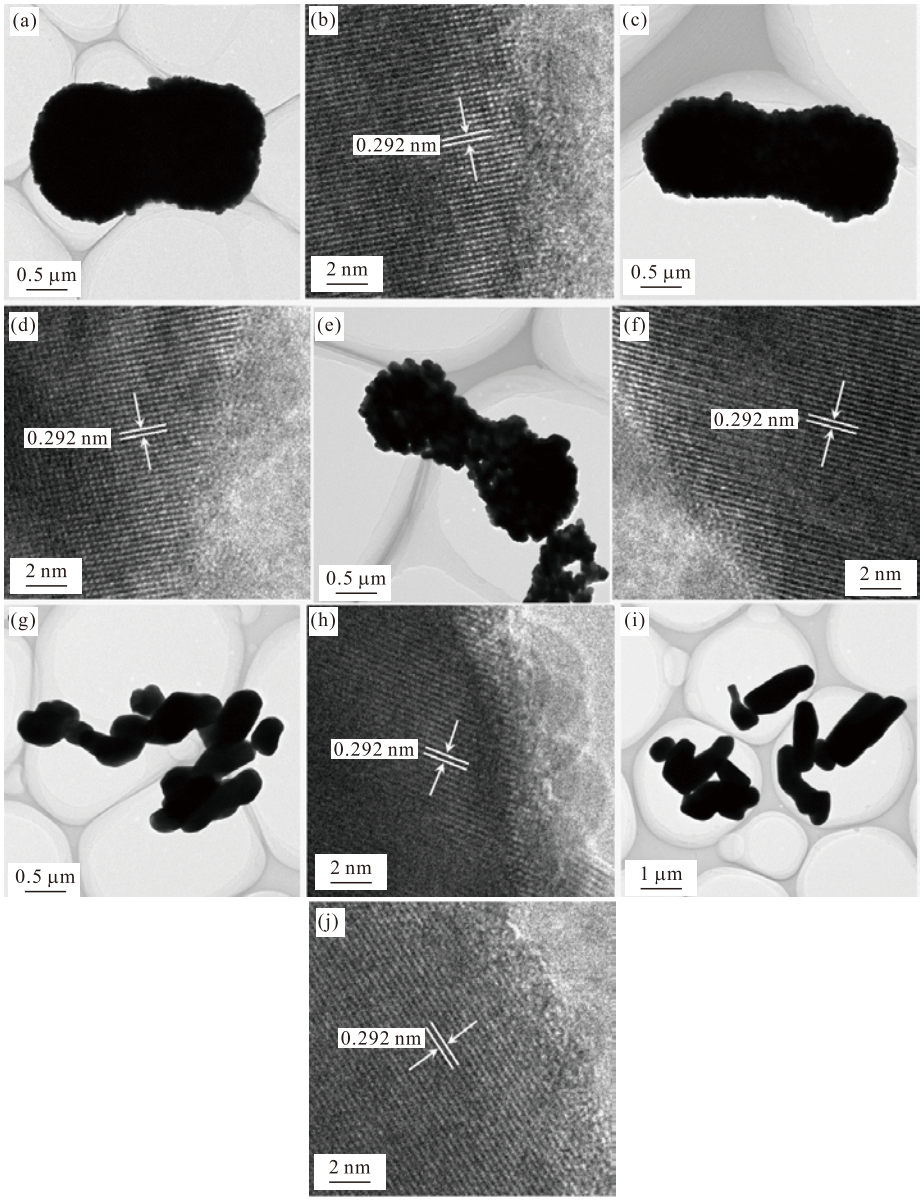

Fig.4 TEM images of the $BiVO_4$ samples synthesized at different pH values: (a-b) pH = 1.68; (c-d) pH = 3.14; (e-f) pH = 4.94; (g-h) pH = 6.87; (i-j) pH = 9.18

of the monomer in the solution. In addition, $NH_3 \cdot H_2O$ could adjust the nucleation rate and crystal growth rate of $BiVO_4$ via a dissolution-recrystallization process. Besides, the growth rate of different facets was distinct, and the blockage induced by OH^- ions attracted on the particle surface[16], the all factors resulted in the morphology evolution. Therefore, the morphology mainly depends on the pH of the precursor.

The BET specific surface area of the $BiVO_4$ samples synthesized at different pH values is summarized in Table 1. It is found that their specific surface area varied as pH values changed, because the samples morphologies depended on the pH values, and the morphology affected the specific surface area[31].

In order to attain detailed information on the microstructures of the $BiVO_4$ samples, TEM was performed, and the results are shown in Fig.4. Figs.4(a), 4(c), and 4(i) display general views of the $BiVO_4$ samples prepared at different pH values, namely N1.68, N3.14, N4.94, N6.87, and N9.18, respectively. The results corresponded to the SEM observation shown in Fig.3. Figs.4(b), 4(d), 4(f), 4(h) and 4(j) show the representative HRTEM images of the samples. The clear lattice fringes presented in each image are indicative of high crystallinity. The lattice spacing of 0.292 nm agrees well with the (040) plane spacing of monoclinic scheelite $BiVO_4$. The HRTEM results are consistent with the information extracted from the XRD patterns, stating that the sample was experiencing morphological changes during the course of pH dictating synthesis, so that (040) plane eventually became the preferential orientation at higher pH value.

3.4 UV-vis diffuse reflectance spectra (UV-vis DRS) performance

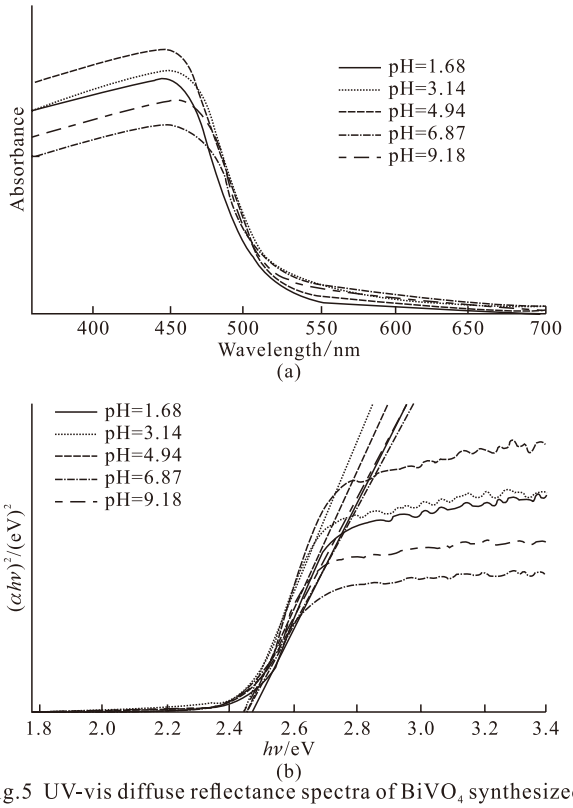

Fig.5 UV-vis diffuse reflectance spectra of $BiVO_4$ synthesized at different pH values

UV-vis diffuse reflectance spectroscopy (UV-vis DRS) is a useful tool for characterizing the electronic states in semiconductor materials[25]. The UV-vis DRS of $BiVO_4$ samples synthesized at different pH values are shown in Fig.5. It can be seen that all the samples exhibit strong absorption in the visible light. The band gap energy can be calculated by the equation $\alpha h\upsilon = A(h\upsilon - E_g)^{1/2}$, where α is the absorption coefficient, $h\upsilon$ is the photon energy, A is a constant (A = 1), and E_g is the band gap energy. The band gap energy can be estimated from a plot of $(\alpha h\upsilon)^2$ versus $h\upsilon$, as shown in Fig.5(b), and the intercept of the tangent to the X-axis gives a good approximation of the band gap energy, and the band gap energies of the samples N1.68, N3.14, N4.94, N6.87 and N9.18 are approximately 2.48, 2.46, 2.45, 2.43, and 2.44 eV, respectively, demonstrating that the electronic structures of samples were changed with the pH varied in the hydrothermal synthesis. The variations in the electronic structures led to different degrees of delocalization of photogenerated carriers, resulting in different mobility efficiency of them. In addition, the electronic structure of the semiconductor usually plays a crucial role in its photocatalytic activity[29], and band gap energy (E_g) is a common feature to evaluate the optical absorption performance of photocatalysts; the lower the E_g value, the higher the photocatalytic performance[28].

3.5 Photocatalytic activity and recycling performance

The photocatalytic performances of $BiVO_4$ samples were investigated by MB degradation under visible light irradiation, and the results are shown in Fig.6. Among all samples, N6.87 exhibits the best MB degradation efficiency, and 100% of MB was degraded after 100 min, while they were 82.7%, 97.9%, 99.3%, and 100% after 120 min in the presence of N1.68, N3.14, N4.94, and N9.18, respectively. Although we should consider the operating parameters when compared with the photocatalytic performances of the others, our results are clearly better than those previously achieved under similar conditions, and the performance of the obtained $BiVO_4$ photocatalysts is higher than that of TiO_2[32] and Bi_2O_3[33].

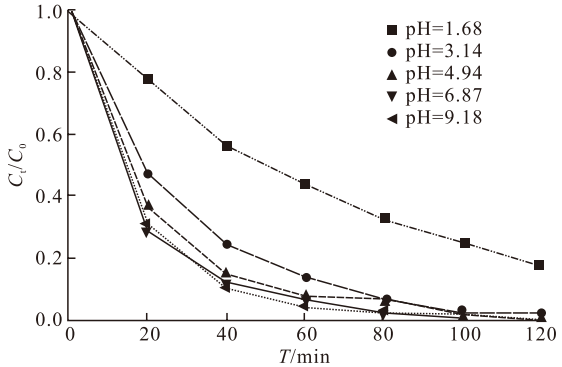

Fig.6 Photocatalytic activity of samples for MB degradation under visible light irradiation

We have determined the surface charge, and the results indicate that the surface charge of all the synthetic $BiVO_4$ samples is negative, and the values are –25.71, –27.94, –30.43, –47.53, and –38.01 mV for N1.68, N3.14, N4.94, N6.87, and N9.18, respectively, as shown in Table 1. Besides, the surface charge of MB is positive, so the MB molecules can adsorb on the $BiVO_4$ particles, which is in favor of MB degradation. In addition, the adsorption capacity is 0.3%, 3.7%, 4.9%, 8.2%, and 6.1% for N1.68, N3.14, N4.94, N6.87, and N9.18, respectively (as shown in Table 1), and the adsorption of MB is a crucial factor for the photocatalysis[34]. From the surface charge and adsorption capacity results, it might be obtained that the surface charge affects the adsorption capacity, and then influences the degradation efficiency. Accordingly, the intensive adsorption of MB should contribute to the high photocatalytic activity.

Furthermore, it is well known that the crystal structure, crystallinity, morphology, surface area and

band gap energy (E_g) of a material are important factors influencing the photocatalytic performance[35,36]. From the XRD results, it is seen that all the $BiVO_4$ samples possess monoclinic crystal structure, indicating that crystal structure does not induce a significant effect in our system. Therefore, the crystallinity, unique morphology, surface area and band gap energy (E_g) would account for the photocatalytic performance. As shown in Table 1, N4.94 possesses the highest surface area (5.01 m^2/g), and the high surface area might supply more active sites for the degradation reaction of MB in aqueous solution, and promotes the electron-hole pairs separation efficiency effectively[37]; N9.18 has the highest degree of crystallinity, and the highly crystalline structure could suppress the recombination of photogenerated electron-hole pairs[31]; N6.87 has rod-like morphology, the lowest band gap energy, the highest surface charge absolute value, and the highest adsorption capacity. These results coincide with their discrepancy in photocatalytic performance, and these observations indicate that the morphology, crystallinity, band gap energy (E_g), BET specific surface area, surface charge and adsorption capacity of the different $BiVO_4$ powders should be considered as affecting the photocatalytic performance together.

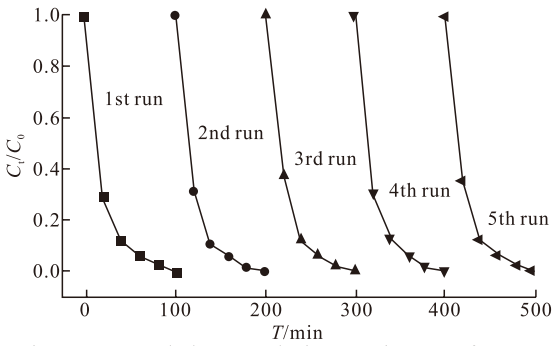

Fig.7 Repeated photocatalytic experiments of N6.87 photocatalyst

The stability and reusability of catalysts are of paramount importance for practical applications. The photo-stability of the synthesized N6.87 photocatalyst was evaluated by the repeated photocatalytic experiments under the same reaction conditions. Fig.7 shows the MB degradation efficiency during each cycle (100 min). The results show that the photocatalyst exhibits no loss of photoactivity after five cycling runs. The N6.87 photocatalyst used in the cycling tests was characterized using SEM and XRD before and after the cycling experiments. The corresponding SEM micrograph (Fig.8(a)) and XRD (Fig.8(b)) results show that the catalysts exhibit no observable changes in the morphologies and crystal structure. These results suggest that the synthetic $BiVO_4$ sample does not suffer from photo corrosion, and has excellent stability and reusability during the degradation process.

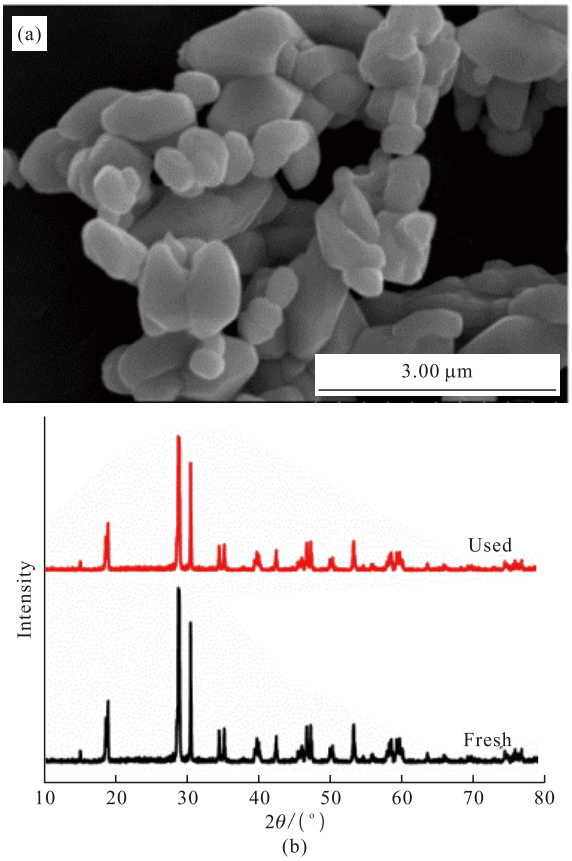

Fig.8 SEM image and XRD patterns of N6.87 sample before and after the photo-stability tests

3.6 Trapping experiments

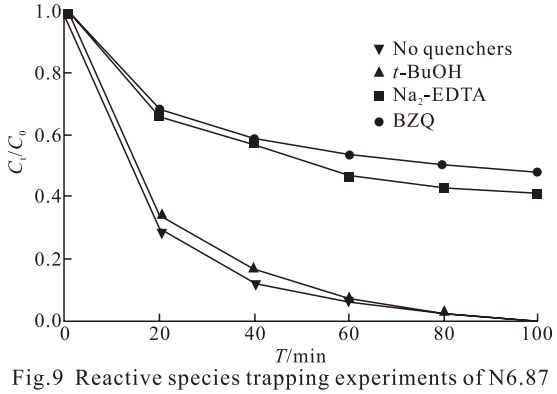

Fig.9 Reactive species trapping experiments of N6.87 photocatalyst

We performed reactive species trapping experiments to detect the main oxidative species (h^+, $\bullet O_2^-$ and •OH) in the photocatalytic reaction to further clarify the photocatalytic mechanism of $BiVO_4$. In this study, tert-butanol (*t*-BuOH, a •OH radical scavenger), p-benzoquinone (BZQ, an $\bullet O_2^-$ radical scavenger), and

disodium ethylene diamine tetra acetate (Na_2-EDTA, a hole scavenger) were used[38]. As shown in Fig.9, the *t*-BuOH had no deleterious effect on the photocatalytic activity, however, the introduction of BZQ reduced the photocatalytic activity from 100% to 58.6% in 100 min, and the presence of Na_2-EDTA also caused deactivation of the N6.87 photocatalyst. These results suggest that h^+ and $\bullet O_2^-$ radicals are the dominant oxidative species in the $BiVO_4$ system, and •OH radicals are not involved.

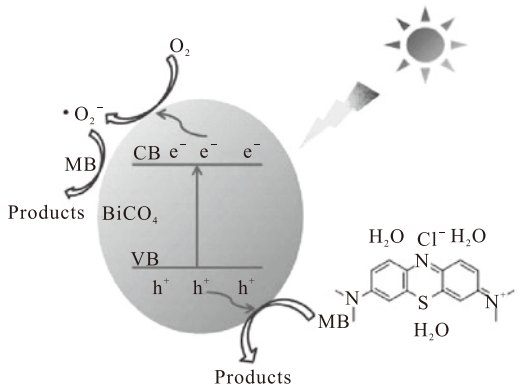

Fig.10 Proposed degradation mechanism of MB by $BiVO_4$ under visible light irradiation

Based on the reactive species trapping experiment results, we conjectured a possible MB photocatalytic degradation mechanism by $BiVO_4$ photocatalysts, as illustrated in Fig.10. Under visible light irradiation, holes (h^+) are generated in the VB, and the electrons (e^-) at the VB are excited to the CB. O_2 molecules adsorbed on the catalyst surface react with e^- to produce $\bullet O_2^-$ radicals, and $\bullet O_2^-$ radicals can degrade MB effectively; h^+ at the VB can oxidize MB directly to degradation production.

4 Conclusions

In summary, $BiVO_4$ samples oriented along (040) crystal facet have been successfully synthesized by a surfactant free hydrothermal method with adjusting the pH values. The results showed that pH values of precursors strongly affected the morphology, crystallinity, band gap energy, BET specific surface area, surface charge and adsorption capacity of powders, and these factors influenced the photocatalytic activities of synthetic $BiVO_4$ samples together. In addition, the $BiVO_4$ photocatalysts have excellent stability and reusability during the degradation process, and photogenerated holes (h^+) and $\bullet O_2^-$ radicals are the predominant oxidative species in the $BiVO_4$ system.

References

[1] Li CJ, Wang SP, Wang T, *et al*. Monoclinic Porous $BiVO_4$ Networks Decorated by Discrete G-C_3N_4 Nano-islands with Tunable Coverage for Highly Efficient Photocatalysis[J]. *Small*, 2014: 1-8

[2] Hu Y, Li D Z, Sun FQ, *et al*. One-pot Template-free Synthesis of Heterophase $BiVO_4$ Microspheres with Enhanced Photocatalytic Activity[J]. *RSC Adv.*, 2015, 5: 54 882-54 889

[3] Gu SN, Li WJ, Wang FZ, *et al*. Synthesis of Buckhorn-like $BiVO_4$ with a Shell of CeO_x Nanodots: Effect of Heterojunction Structure on the Enhancement of Photocatalytic Activity[J]. *Appl. Catal. B: Environ.*, 2015, 170-171: 186-194

[4] Obregón S, Colón G. Heterostructured Er^{3+} Doped $BiVO_4$ with Exceptional Photocatalytic Performance by Cooperative Electronic and Luminescence Sensitization Mechanism[J]. *Appl. Catal. B: Environ*., 2014, 158-159: 242-249

[5] Li JQ, Cui MM, Liu ZX, *et al*. $BiVO_4$ Hollow Spheres with Hierarchical Microstructures and Enhanced Photocatalytic Performance under Visible-light Illumination[J]. *Phys. Status Solidi A*, 2013, 9: 1 881-1 887

[6] Zhang ZJ, Wang WZ, Shang M, *et al*. Photocatalytic Degradation of Rhodamine B and Phenol by Solution Combustion Synthesized $BiVO_4$ Photocatalyst[J]. *Catal. Commun.*, 2010, 11: 982-986

[7] Fan HM, Jiang TF, Li HY, *et al*. Effect of $BiVO_4$ Crystalline Phases on the Photoinduced Carriers Behavior and Photocatalytic Activity[J]. *J. Phys. Chem. C*, 2012, 116: 2 425-2 430

[8] Tokunaga S, Kato H, Kudo A. Selective Preparation of Monoclinic and Tetragonal $BiVO_4$ with Scheelite Structure and Their Photocatalytic Properties[J]. *Chem. Mater*., 2001, 13: 4 624-4 628

[9] Cheng B, Wang WG, Shi L, *et al*. One-pot Template-free Hydrothermal Synthesis of Monoclinic $BiVO_4$ Hollow Microspheres and Their Enhanced Visible-light Photocatalytic Activity[J]. *Int. J. Photoenergy*, 2012: 1-10

[10] Shen Y, Huang ML, Huang Y, *et al*. The Synthesis of Bismuth Vanadate Powders and Their Photocatalytic Properties under Visible Light Irradiation[J]. *J. Alloys Compd.*, 2010, 496: 287-292

[11] Ke DN, Peng TY, Ma L, *et al*. Effects of Hydrothermal Temperature on the Microstructures of $BiVO_4$ and Its Photocatalytic O_2 Evolution Activity under Visible Light[J]. *Inorg. Chem.*, 2009, 48: 4 685-4 691

[12] Xu J, Wang WZ, Wang J, *et al*. Controlled Fabrication and Enhanced Photocatalystic Performance of $BiVO_4$@CeO_2 Hollow Microspheres for the Visible-light-driven Degradation of Rhodamine B[J]. *Appl. Surf. Sci.*, 2015, 349: 529-537

[13] Jiang HY, Meng X, Dai HX, *et al*. High-performance Porous Spherical or Octapod-like Single-crystalline $BiVO_4$ Photocatalysts for the Removal of Phenol and Methylene Blue under Visible-light Illumination[J]. *J. Hazard. Mater*., 2012, 217-218: 92-99

[14] Thalluri SM, Hussain M, Saracco G, *et al*. Green-synthesized $BiVO_4$ Oriented Along {040} Facets for Visible Light-driven Ethylene Degradation[J]. *Ind. Eng. Chem. Res*., 2014, 53: 2 640-2 646

[15] Eda S, Fujishima M, Tada H. Low Temperature-synthesis of $BiVO_4$

Nanorods Using Polyethylene Glycol as a Soft Template and the Visible-light-activity for Copper Acetylacetonate Decomposition[J]. *Appl. Catal. B: Environ*., 2012, 125: 288-293

[16] Dong SY, Feng JL, Li YK, *et al*. Shape-controlled Synthesis of $BiVO_4$ Hierarchical Structures with Unique Natural-sunlight-driven Photocatalytic Activity[J]. *Appl. Catal. B: Environ*., 2014, 152-153: 413-424

[17] Sun JH, Yang H. A Polyacrylamide Gel Route to Photocatalytically Active $BiVO_4$ Particles with Monoclinic Scheelite Structure[J]. *Ceram. Int.*, 2014, 40: 6 399-6 404

[18] Jiang HY, Dai HX, Meng X, *et al*. Hydrothermal Fabrication and Visible- light-driven Photocatalytic Properties of Bismuth Vanadate with Multiple Morphologies and/or Porous Structures for Methyl Orange Degradation[J]. *J.Environ. Sci.*, 2012, 3: 449-457

[19] García-Péreza UM, Martínezde la Cruzb A, Sepúlveda-Guzmánb S, Peral J. Low-temperature Synthesis of $BiVO_4$ Powders by Pluronic-Assisted Hydrothermal Method: Effect of the Surfactant and Temperature on the Morphology and Structural Control[J]. *Ceram. Int.*, 2014, 40: 4 631-4 638

[20] Li F, Yang CY, Li QG, *et al*. The pH-controlled Morphology Transition of $BiVO_4$ Photocatalysts from Microparticles to Hollow Microspheres [J]. *Mater. Lett*., 2015, 145: 52-55

[21] Sun SM, Wang WZ, Zhou L, *et al*. Efficient Methylene Blue Removal Over Hydrothermally Synthesized Starlike $BiVO_4$[J]. *Ind. Eng. Chem. Res*., 2009, 48: 1 735-1 739

[22] Shen Y, Huang M, Huang Y, *et al*. The Synthesis of Bismuth Vanadate Powders and Their Photocatalytic Properties under Visible Light Irradiation[J]. *J. Alloys Compd*., 2010, 496: 287-292

[23] Shang M, Wang WZ, Ren J, *et al*. A Novel $BiVO_4$ Hierarchical Nanostructure: Controllable Synthesis, Growth Mechanism, and Application in Photocatalysis[J]. *Cryst. Eng. Comm*., 2010, 12: 1 754-1 758

[24] Obregón S, Caballero A, Colón G. Hydrothermal Synthesis of $BiVO_4$: Structural and Morphological Influence on the Photocatalytic Activity [J]. *Appl. Catal. B: Environ*., 2012, 117-118: 59-66

[25] Yu JQ, Kudo A. Effects of Structural Variation on the Photocatalytic Performance of Hydrothermally Synthesized $BiVO_4$[J]. *Adv. Funct. Mater.*, 2006, 16: 2 163-2 169

[26] Ai ZH, Lee SC. Morphology-dependent Photocatalytic Removal of NO by Hierarchical $BiVO_4$ Microboats and Microspheres under Visible Light[J]. *Appl. Surf. Sci*., 2013, 280: 354-359

[27] Kho YK, Teoh WY, Iwase A, *et al*. Flame Preparation of Visible-light-Responsive $BiVO_4$ Oxygen Evolution Photocatalysts with Subsequent Activation Via Aqueous Route[J]. *ACS Appl. Mater. Inter.*, 2011, 3: 1 997-2 004

[28] Yao MM, Liu MX, Gan LH, *et al*. Monoclinic Mesoporous $BiVO_4$: Synthesis and Visible-light-driven Photocatalytic Property[J]. *Colloids Surf. A: Physicochem. Eng. Aspects*, 2013, 433: 132-138

[29] Zhang AP, Zhang JZ, Cui NY, *et al*. Effects of pH on Hydrothermal Synthesis and Characterization of Visible-light-driven $BiVO_4$ Photocatalyst[J]. *J. Mol. Catal. A-Chem.*, 2009, 304: 28-32

[30] Zhou B, Zhao X, Liu HJ, Qu J, *et al*. Synthesis of Visible-light Sensitive M-$BiVO_4$ (M = Ag, Co, and Ni) for the Photocatalytic Degradation of Organic Pollutants[J]. *Separ. Purif. Tech.*, 2011, 77: 275-282

[31] Zhou Y, Vuille K, Heel A, *et al*. An Inorganic Hydrothermal Route to Photocatalytically Active Bismuth Vanadate[J]. *Appl. Catal. A: Gene*., 2010, 375: 140-148

[32] Wen LP, Liu BS, Liu C, *et al*. Preparation, Characterization and Photocatalytic Property of Ag-loaded TiO_2 Powders Using Photodeposition Method[J]. *Journal of Wuhan University of Technology-Mater. Sci. Ed*., 2008, 24(2): 258-263

[33] Guo WF, Li HP, Teng WX, *et al*. Effect of the pH Value of Synthesis Conditions on the Phase Structure and Photocatalytic Properties of Bismuth Molybdates Synthesized Using a Hydrothermal Method[J]. *Nanomater. Nanotechnol*., 2015, 5:24

[34] Lei LW, Jin HH, Zhang Q, *et al*. A Novel Enhanced Visible-light-driven Photocatalyst Via Hybridization of Nanosized BiOCl and Graphitic C_3N_4[J]. *Dalton Trans.*, 2015, 44: 795-803

[35] Jiang HY, Dai HX, Meng X, *et al*. Porous Olive-like $BiVO_4$: Alcoho-hydrothermal Preparation and Excellent Visible-light-driven Photocatalytic Performance for the Degradation of Phenol[J]. *Appl. Catal. B: Environ.*, 2011, 105: 326-334

[36] Meng X, Zhang L, Dai HX, *et al*. Surfactant-assisted Hydrothermal Fabrication and Visible-light-driven Photocatalytic Degradation of Methylene blue Over Multiple Morphological $BiVO_4$ Single-crystallites[J]. *Mater. Chem. Phys*., 2011, 125: 59-65

[37] Li GS, Zhang DQ, Yu JC. Ordered Mesoporous $BiVO_4$ Through Nanocasting: a Superior Visible Light-driven Photocatalyst[J]. *Chem. Mater.*, 2008, 20: 3 983-3 992

[38] Yang XF, Cui HY, Li Y, *et al*. Fabrication of Ag_3PO_4-graphene Composites with Highly Efficient and Stable Visible Light Photocatalytic Performance[J]. *ACS Catal*., 2013, 3: 363-369